Proceedings of the ASME 2015 International Mechanical Engineering Congress and Exposition
IMECE 2015
November 13 – 19, 2015, Houston, Texas, USA

IMECE2015-50423

AN EXTENDED FINITE ELEMENT MODEL OF CREVICE AND PITTING CORROSION

Ravindra Duddu
Department of Civil and Environmental Engineering
Vanderbilt University
Nashville, TN 37212
Email: ravindra.duddu@vanderbilt.edu

Nithyanand Kota
Materials, Corrosion and Engineering Technologies (MCET)
Leidos Corporation
Arlington, VA 22203
Email: nithyanandkota@gmail.com

Siddiq Qidwai
Multifunctional Materials Branch, Code 6350
U.S. Naval Research Laboratory
Washington, DC 20375
Email: siddiq.qidwai@nrl.navy.mil

ABSTRACT

A sharp interface model formulation is developed for simulating the electrochemical environment in crevices/pits due to galvanic corrosion in aqueous media. The concentration of ionic species and the electrical potential in the crevice is established using the non-dimensionalized Nernst-Planck equations along with the assumption of local electro-neutrality. The crevice/pit interface fluxes are defined in terms of the cathodic and anodic current densities using Butler-Volmer kinetics. The extended finite element method is used to discretize the governing equations and the level set function to describe the interface morphology independent of the underlying finite element mesh. The advantage of this formulation is that it eliminates the need for cumbersome mesh generation and remeshing when the interface morphology changes. Numerical investigations of steady-state intergranular crevice corrosion in idealized Al-Mg alloy microstructures in two-dimensions are conducted to establish the viability of the formulation. Simulation results predict large pH and chloride concentration within the crevice environment, which leads us to the conclusion that chemical reactions and precipitation play a prominent role during crevice corrosion.

INTRODUCTION

Crevice and pitting corrosion are forms of localized corrosion in alloys of stainless steel and aluminum that are otherwise resistant to uniform corrosion. Pits and crevices formed by localized corrosion in structural components provide ideal locations for the nucleation of fatigue cracks [1] that can eventually lead to catastrophic failure of the component and or the entire structure; therefore, it is important that we investigate and understand the physical mechanisms of crevice and pit growth in corrosive environments. To this end, an extended finite element method (XFEM) based model formulation is developed in this paper for simulating the electrochemical environment in crevices and pits due to galvanic corrosion in aqueous media in two-dimensions (2-D). The proposed mechanistic (physics-based) model formulation is a first step towards simulating the propagation of corrosion crevices and pits in an accurate and computationally efficient manner.

It is well known that corrosion of metals and alloys proceeds due to galvanic action [2], an extremely complex electrochemical process, that depends on compositional variables (e.g. alloying elements, intermetallic particles, oxide film, perforated cover), environmental variables of the pit solution (e.g. pH, Chloride concentration, dissolved ionic species, reaction products, temperature), and processing variables (e.g. grain structure, thermo-mechanical processing, surface wear). Due to the complexity and inherent unpredictability in the initiation and propagation events, localized corrosion is a very difficult phenomenon and continues to evade our understanding [3]. Mathematical and computational modeling of corrosion along with controlled or accelerated laboratory experiments can yield considerable insights into the roles of the various compositional, environmental and processing variables on the corrosion behavior of alloys. Such insights can then lead us towards the development of better processing techniques or design of microstructure. In this context, mechanistic (physics-based) models of corrosion propagation based on mass and charge balance equations in multi-phase domains can provide great opportunity; however, they present significant mathematical and numerical challenges.

The simplest formulation of the mechanistic models of corrosion propagation considers metal dissolution to be governed only by diffusive mass transport [4–6]. For the sake of corrosion propagation modeling, it is a common practice to assume that corrosion pit has already nucleated and that the

initial shape of the corrosion pit is semicircular in 2-D (or hemispherical in 3-D). In this model, corrosion propagation can be either activation-controlled (i.e., the corrosion current density determines the rate of propagation) or diffusion-controlled (i.e., the saturation limit of dissolved metal ion concentration determines the rate of propagation). These two scenarios lead to widely different corrosion pit growth behaviors in that activation-controlled corrosion generally preserves the initial pit morphology giving rise to narrow deep pits, whereas, diffusion-controlled corrosion smoothens the initial shape giving rise to semi-circular or wide semi-elliptical pits [7, 8]. Despite the success of the Fickian diffusion based mass transport models in capturing pitting corrosion growth in stainless steel alloys; these models are not generally suitable because they ignore the electro-chemical aspects of galvanic corrosion in alloys.

Perhaps, the first-ever comprehensive mechanistic model of crevice and pitting corrosion was proposed in [9]. This model considered not only the diffusion of ions due to concentration gradients but also electro-migration of dissolved ionic species in the aqueous solution environment within the pit or crevice and the rate of depletion or production of ions due to chemical reactions for investigating corrosion in stainless steel alloys. The electro-diffusion of ions was modeled based on dilute solution theory using the Nernst-Planck equations along with the assumption of local electro-neutrality. However, owing to its computational complexity, this class of models was only used to investigate 1-D crevice corrosion propagation [3, 9–11]. Due to the recent advances in computing platforms and the emergence of robust commercial software such as COMSOL, there has been a renewed interest in comprehensive mechanistic modeling of corrosion. Several recent studies followed the dilute solution theory approach to simulate and investigate corrosion in various aluminum and steel alloys [12–18].

Despite the availability of advanced computing resources and software, simulating pit or crevice corrosion propagation persists to be an extremely challenging problem because it involves tracking a moving electrode-electrolyte boundary (interface) across which the concentrations of ions and their gradients are discontinuous (sharp-interface assumption). The need to solve non-linear second-order partial differential equations associated with electro-diffusive transport in the electrolyte domain and with propagating interfaces present formidable challenges for both sharp interface approaches [8, 19, 20] and diffuse interface approaches [21]. One of the major computational challenges with sharp-interface models is that the standard finite element method cannot capture the interfacial discontinuities within a finite element and would necessitate remeshing every time the interface morphology changes, which can be cumbersome. Methods such as arbitrary Eulerian-Lagrangian, meshfree/meshless, or moving mesh for evolving sharp interfaces can be tedious and/or computationally expensive, especially, when Neumann and Dirichlet boundary conditions are prescribed on the interface.

To address the above computational challenge, herein, a new extended finite element formulation is developed for describing the corrosion behavior of arbitrarily shaped crevices/pits using a simple structured finite element mesh. By enriching the standard finite element approximation space with the Heaviside function, the discontinuity or jump in the value of the concentration fields or their gradients can be incorporated across the embedded interface. The main advantage is that the XFEM eliminates the need for remeshing when the interface morphology changes. While, the XFEM was previously employed to simulate diffusion-controlled corrosion pit propagation [8, 20], the formulation proposed herein is novel in that it is based on the dilute solution theory for ion diffusion instead of Fickian diffusion. The variational formulation of the Nernst-Planck equations allows for the imposition of boundary conditions on an arbitrary sharp interface, without any difficulty. Numerical investigations of steady-state intergranular crevice corrosion in idealized Al-Mg alloy microstructures in two-dimensions, presented herein. Two different crevice interface morphologies are considered to establish the ability of the XFEM to investigate the physics of corrosion.

NOMENCLATURE

Roman

a_i^B	Enrichment degrees of freedom corresponding to i^{th} ionic species concentration at an enriched node B
C_i	Concentration of the i^{th} ionic species in aqueous solution [mol/m^3]
C_0	Reference concentration for normalization [mol/m^3]
c_i	Non-dimensionalized concentration of i^{th} ionic species in aqueous solution
c_i^∞	Far-field concentration of the i^{th} ionic species in aqueous solution [mol/m^3]
D_i	Fickian diffusion coefficient of i^{th} ionic species in aqueous solution [m^2/s]
D_0	Reference diffusion coefficient for normalization
F	Faraday's constant [C/mol]
f	Phase volume fraction of aluminum in the alloy
i	Corrosion current density [A/m^2]
$\boldsymbol{j}_i$	Non-dimensionalized flux density corresponding to i^{th} ionic species concentration
$\boldsymbol{j}_\psi$	Non-dimensionalized flux density corresponding to the electrical potential
K_{sp}	Solubility product of $Mg(OH)_2$ at 25 °C
L_0	Reference length scale for normalization [m]
N^A	Standard finite element shape function at node A
$\boldsymbol{n}$	Unit normal vector to the solid-liquid interface pointing towards the liquid domain
n_e	Total number of enriched finite element nodes
n_s	Total number of finite element nodes in the mesh
R	Universal gas constant [J/mol/K]
r_i	Chemical reactions corresponding to the i^{th} ionic

	species in aqueous solution
S^B	Step enrichment function at node B
T	Temperature of the system [K]
t	Time [s]
$\boldsymbol{x}$	Spatial Cartesian system of coordinates in 2-D {[m],[m]}
z_i	Charge number of the i^{th} ionic species in aqueous solution

Greek

β	Tafel constant for the electrode reaction
Γ_{int}	Solid-liquid (electrode-electrolyte) interface
Γ	Domain boundary or interface
φ	Electrical potential in the solution domain [V]
ϕ	Level set function
ψ	Non-dimensionalized electrical potential
Ω_l	Liquid (aqueous solution) domain
Ω_s	Solid alloy domain

Subscripts

a	Anode
c	Cathode
e	External
f	Forward
h	Finite element mesh (size) parameter
o	Open circuit
r	Reverse

MODEL FORMULATION

In this section, the governing equations of the mathematical model of intergranular crevice corrosion in aluminum alloys AA5083 are detailed. The procedure for the derivation of the strong form of the model follows closely the formulation of Sharland et al., [3]. The domain set up is similar to that described in Sarkar et al., [16]; however, the present model considers four ionic species including $Cl^-$and Na^+ as opposed to only two ionic species Mg^{2+} and OH^-. While the model is developed for crevice corrosion, it would also be applicable for studying pitting corrosion. As Sharland et al., [13] remarked, "From the electrochemical point of view, it has been suggested that both processes (i.e., crevice and pitting corrosion) are identical but crevice corrosion involves longer ionic diffusion path."

Domain Description

Herein, the crevice corrosion problem is reduced to two-dimensions (2-D) by considering uniformity in the out of plane direction. Let us consider a rectangular domain $\Omega = \Omega_s \cup \Omega_l$ that consists of two phases: the solid alloy domain $\Omega_s(t)$ and the liquid solution domain $\Omega_l(t)$ at all times t, as shown in Figure 1. The solid and liquid domains are separated by a sharp evolving interface $\Gamma_{int} = \Gamma_c \cup \Gamma_a$ that is the union of the cathode surface $\Gamma_c(t)$ and anode surface $\Gamma_a(t)$. The interface Γ_{int} is implicitly defined using a level set function ϕ as,

$$\Gamma_{int} = \{\boldsymbol{x} \in \Omega \mid \phi(\boldsymbol{x}, t) = 0\} \quad (1)$$

where $\boldsymbol{x}$ denotes the spatial Cartesian system of coordinates and $\phi > 0$ in Ω_l and $\phi < 0$ in Ω_s, by definition. As corrosion progresses, Γ_a moves downward and Γ_c increases due to the exposed sidewalls. The solid domain is composed of a binary Aluminum-Magnesium (Al-Mg) alloy, wherein the Mg phase is anodic with respect to the Al phase. A volume fraction (phase) variable $f(\boldsymbol{x})$ is introduced to capture the spatial distribution of Al and Mg phases in the solid alloy domain, such that, $f = 1$ in the Al phase and $f = 0$ in the Mg phase. For the sake of this study, the microstructure of AA5083 is idealized to consist two square shaped grains of Al phase (light grey) separated by the grain boundary region consisting of Mg phase (dark grey), as shown in Figure 1. The alloy is immersed in 0.5M NaCl aqueous solution and the concentrations of four ionic species Mg^{2+}, OH^-, Na^+ and Cl^- in solution are tracked.

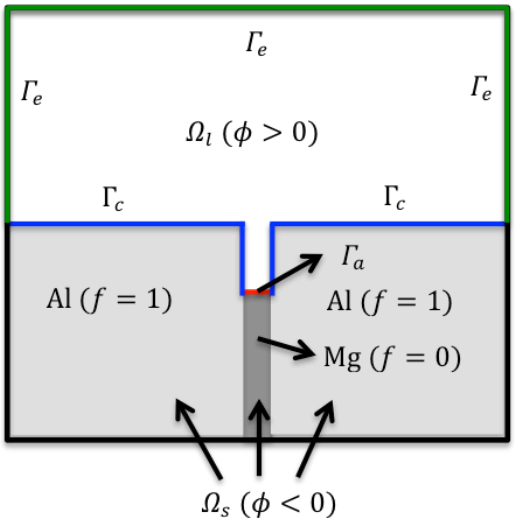

Figure 1. Schematic diagram of the intergranular crevice corrosion problem in the Al-Mg (AA5083) alloy system. The union of the cathodic (blue) and anodic (red) surfaces defines the sharp interface between the solid domain and the liquid (aqueous) domain. Beyond the external boundary (green) far field concentrations are assumed.

Corrosion kinetics

Intergranular crevice corrosion in AA5083 alloys occurs due to galvanic action at the interface Γ_{int}, wherein the surface of the Mg phase exposed to NaCl solution acts as the anode and exposed surface of the Al phase acts as the cathode. As an electric current is established between the anode and cathode regions, corrosion quickly progresses due to the dissolution of Mg into aqueous solution as Mg^{2+} ions at the anode boundary Γ_a. Thus, the anodic reaction involves oxidation of Mg as,

$$\mathrm{Mg} \underset{\beta_{ar}}{\overset{\beta_{af}}{\rightleftarrows}} \mathrm{Mg}^{2+} + 2e^- \tag{2}$$

and the cathodic reaction involves reduction of water as,

$$2\mathrm{H_2O} + \mathrm{O_2} + 4e^- \underset{\beta_{cr}}{\overset{\beta_{cf}}{\rightleftarrows}} 4\mathrm{OH}^- \tag{3}$$

where β_{af}, β_{ar}, β_{cf} and β_{cr} are the forward and reverse Tafel constants for the anodic and cathodic reactions, respectively. The current densities at the anode and cathode surfaces are defined in accordance with Bulter-Volmer kinetics as [18],

$$i_a = i_{oa}\left[10^{\left(\frac{\varphi-\varphi_{oa}}{\beta_{af}}\right)} - 10^{\left(\frac{\varphi-\varphi_{oa}}{\beta_{ar}}\right)}\right] \text{ on } \Gamma_a \tag{4}$$

$$i_c = i_{oc}\left[10^{\left(\frac{\varphi-\varphi_{oc}}{\beta_{cf}}\right)} - 10^{\left(\frac{\varphi-\varphi_{oc}}{\beta_{cr}}\right)}\right] \text{ on } \Gamma_c \tag{5}$$

where i_{oa} and i_{oc} are the anodic and cathodic open-circuit current densities, and φ_{oa} and φ_{oc} are the corresponding open-circuit electrical potentials.

Strong form of governing equations

The steady-state concentrations of ionic species in aqueous solution along with the local electro-neutrality condition for electrical potential ψ in $\Omega_l(t)$ are given by the Nernst-Planck equations in the non-dimensionalized form as [3],

$$\nabla \cdot (\nabla c_i + z_i c_i \nabla \psi) = r_i \quad i = \{1,2,3,4\} \tag{6}$$

$$\sum_{i=1}^{4} \frac{D_0 c_i z_i}{D_i} = 0 \tag{7}$$

where $c_i = \frac{D_i C_i}{D_0 C_0}$ is the non-dimensionalized concentration, D_i [m^2/s] is the Fickian diffusion coefficient, C_i [mol/m^3] is the concentration, z_i is the charge number, and r_i is the chemical reaction term associated with the i^{th} species in the aqueous solution; D_0 [m^2/s] and C_0 [mol/m^3] are chosen constants for non-dimensionalization, $\psi = \frac{F\varphi}{RT}$ is the non-dimensionalized electrical potential, φ [V] is the electrical potential, F [C/mol] is the Faraday's constant, R [J/mol/K] is the universal gas constant and T [K] is the temperature.

For this study, we consider four ionic species, c_1, c_2, c_3, c_4 denoting the concentrations of Mg^{2+}, OH^-, $Cl^-$and Na^+, respectively. The chemical reaction occurring between Mg^{2+} and OH^- that leads to the formation of magnesium hydroxide $Mg(OH)_2$ is ignored, that is, $r_i = 0$, which is a very critical and significant assumption. While, it should be relatively straightforward to incorporate reactions terms into the present formulation, the forward and backward reaction rate constants for the precipitation and dissolution of $Mg(OH)_2$ are not adequately reported in the literature. Alternatively, the ion diffusion equation corresponding to OH^- concentration can be replaced with the equilibrium (solubility product) calculation taking $K_{sp} = 1.8 \times 10^{-11}$ for $Mg(OH)_2$, similar to the model in [9]; however, such a model cannot be implemented in COMSOL, so validation is difficult. Since the aim of this study is to establish the validity of the proposed extended finite element model formulation, chemical reactions associated with the precipitation of $Mg(OH)_2$ are ignored.

Notice that while equation (7) establishes the electrical potential ψ, it does not contain a ψ term; so this leads to zero values on the diagonal of the system tangent matrix. Thus, the discretization of the above equations (6) and (7) could lead to numerical convergence issues due to poor conditioning of the matrix. In order to alleviate this ill-conditioning, the linear system of equations can rearranged as follows:

$$\nabla \cdot (\nabla c_i + z_i c_i \nabla \psi) = 0 \text{ in } \Omega_l \;\; i = \{1,2,3\} \tag{8}$$

$$\sum_{i=1}^{4} \frac{D_0 c_i z_i}{D_i} = 0 \text{ in } \Omega_l \tag{9}$$

$$\sum_{i=1}^{4} \nabla \cdot (z_i \nabla c_i + z_i^2 c_i \nabla \psi) = 0 \text{ in } \Omega_l \tag{10}$$

The above equation (10) is obtained by summing the four equations defined by equation (6) with $r_i = 0$. Thus, the concentration of Na^+ (c_4) is evaluated using the electro-neutrality equation (9) rather than the Nernst-Planck equation (6), whereas, equation (10) is used to establish ψ. This rearrangement of the equations leads to improved numerical convergence due to a better conditioning of the tangent matrix.

Equations (8) and (10) are subject to boundary conditions, which will complete the description of the strong form of the governing equations. The three equations described by (8) are constrained by Dirichlet conditions on the external boundary Γ_e (green) and Neumann conditions on the anodic (red) and cathodic (green) boundaries as given by,

$$\begin{gathered} c_i = c_i^{\infty} \text{ on } \Gamma_e \\ \boldsymbol{j}_1 \cdot \boldsymbol{n} = \frac{i_a L_0}{z_1 F D_0 C_0} \text{ and } \boldsymbol{j}_2 \cdot \boldsymbol{n} = \boldsymbol{j}_3 \cdot \boldsymbol{n} = 0 \text{ on } \Gamma_a \\ \boldsymbol{j}_1 \cdot \boldsymbol{n} = \boldsymbol{j}_3 \cdot \boldsymbol{n} = 0 \text{ and } \boldsymbol{j}_2 \cdot \boldsymbol{n} = \frac{i_c L_0}{z_2 F D_0 C_0} \text{ on } \Gamma_c \end{gathered} \tag{11}$$

In the above equation (11), $\boldsymbol{n}$ denotes the unit normal to the interface Γ_{int} pointing towards Ω_l, L_0 is a reference length scale for normalizing the molar flux, c_i^{∞} denotes the bulk or far field concentration of the i^{th} ionic species and $\boldsymbol{j}_i$ denotes the flux corresponding to c_i defined as,

$$\boldsymbol{j}_i = -(\nabla c_i + z_i c_i \nabla \psi) L_0 \tag{12}$$

Equation (9) is the electro-neutrality constraint that should be enforced everywhere in the domain including the boundaries. Equation (10) is subject to Neumann (flux) boundary conditions on the anode and cathode boundaries as given by,

$$\boldsymbol{j}_{\psi} \cdot \boldsymbol{n} = \frac{i_{a/c} L_0}{F C_0 D_0} \text{ on } \Gamma_{a/c} \tag{13}$$

where the flux corresponding to the potential ψ is defined as,

$$\boldsymbol{j}_{\psi} = \sum_{i=1}^{4} (z_i \nabla c_i + z_i^2 c_i \nabla \psi) L_0 \tag{14}$$

Equations (8)–(10) along with boundary conditions described in equations (11) and (13) and corrosion kinetic relations in equations (4) and (5) establish the strong form of the governing equations of the crevice corrosion problem.

Weak form of governing equations

The variational or weak form corresponding to equation (8) can be stated as:

Find $c_i \in \mathcal{C}$ $(i = \{1,2,3\})$ for all $w \in \mathcal{W}$ such that,

$$\begin{aligned} &\int_{\Gamma_{int}} w \, \nabla c_i \cdot \boldsymbol{n} \, \mathrm{d}\Omega + \int_{\Gamma_{int}} w z_i c_i \nabla \psi \cdot \boldsymbol{n} \, \mathrm{d}\Omega \\ &\quad - \int_{\Omega_l} \nabla w \cdot \nabla c_i \, \mathrm{d}\Omega - \int_{\Omega_l} \nabla w \cdot (\nabla \psi z_i c_i) \, \mathrm{d}\Omega = 0 \end{aligned} \tag{15}$$

Substituting the relations for the flux in (12) and the boundary conditions in (11) into the above equation, the final form the weak form can be obtained as,

$$\int_{\Gamma_{int}} w \frac{1}{L_0} \boldsymbol{j}_i \cdot \boldsymbol{n} \, \mathrm{d}\Omega - \int_{\Omega_l} \nabla w \cdot (\nabla c_i + \nabla \psi z_i c_i) \mathrm{d}\Omega \tag{16}$$

The weak form corresponding to equation (9) is given by,

Find $c_4 \in \mathcal{C}$ such that,

$$\int_{\Omega_l \cup \Gamma_{int}} w \sum_{i=1}^{4} \frac{D_0 c_i z_i}{D_i} = 0 \tag{17}$$

Finally, the weak form of corresponding to equation (10) is,

Find $\psi \in \Psi$ for all $u \in \mathcal{U}$ such that,

$$\begin{aligned} &\int_{\Gamma_{int}} u \frac{1}{L_0} \boldsymbol{j}_{\psi} \cdot \boldsymbol{n} \, \mathrm{d}\Omega \\ &\quad - \int_{\Omega_l} \nabla u \cdot \sum_{i=1}^{4} (z_i \nabla c_i + z_i^2 c_i \nabla \psi) = 0 \end{aligned} \tag{18}$$

Note that in above three equations the $\mathcal{C}, \Psi, \mathcal{U}$ and $\mathcal{W}$ are spaces of sufficiently smooth functions for the respective bulk fields and their variations, and w, u denote the test functions.

NUMERICAL IMPLEMENTATION

In this section, the extended finite element method (XFEM) and its implementation are detailed for the crevice corrosion problem. Belytschko and co-workers [22,23] originally proposed the XFEM so as to simulate crack propagation with minimal remeshing. The XFEM is generally coupled with the level set method [24] to represent the embedded interface, independent of the underlying finite element mesh.

Extended finite element approximation

Let Ω^h represent the discretization of the entire computational domain Ω, wherein the physical domain is divided into finite elements and the superscript h denotes the mesh parameter. In this problem, there are five unknown fields to be described on Ω^h: the non-dimensionalized ionic species concentrations c_1 (Mg^{2+}), c_2 (OH^-), c_3 (Cl^-), c_4 (Na^+) and the electrical potential ψ. Since these unknown fields are only defined in the liquid (aqueous solution) domain, from a mathematical perspective, these unknown fields can be defined as zero valued in the solid (alloy) domain; consequently, there exists a jump or discontinuity in the value of these unknown fields at the interface Γ_{int}. Thus, in the proposed extended finite element formulation the unknown fields are approximated as,

$$c_i^h(\boldsymbol{x}, t) = \sum_{A=1}^{n_s} N^A(\boldsymbol{x}) \, c_i^A(t) + \sum_{B=1}^{n_e} S^B(\boldsymbol{x}, t) \, a_i^B(t) \tag{19}$$

$$\psi^h(\boldsymbol{x}, t) = \sum_{A=1}^{n_s} N^A(\boldsymbol{x}) \, \psi^A(t) + \sum_{B=1}^{n_e} S^B(\boldsymbol{x}, t) \, \xi^B(t) \tag{20}$$

where N^A denotes the standard finite element shape functions, c_i^A and ψ^A denoted the nodal degrees of freedom (DOFs) corresponding to the non-dimensionalized concentration of the i^{th} ionic species and electrical potential at node A, respectively, n_s is the total number of nodes in the mesh, a_i^B and ξ^B are the nodal enrichment DOFs (which are additional DOFs at the enriched nodes) corresponding to c_i^A and ψ^A at enriched node B, $n_e(t)$ is the total number of enriched nodes in the mesh at time t, and the step enrichment function corresponding to enriched node B is defined as,

$$S^B(\boldsymbol{x}, t) = N^B(\boldsymbol{x})(H(\phi(\boldsymbol{x}, t) - H(-\phi(\boldsymbol{x}, t))) \tag{21}$$

In the above equation, the Heaviside function is defined as $H(\phi) = 1$ if $\phi > 0$ and $H(\phi) = 0$ if $\phi < 0$. The enrichment function $S^B(\boldsymbol{x}, t)$ allows for the discontinuity in the unknown fields at the interface Γ_{int}. Since the level set function ϕ is not

discontinuous across the interface, it can be approximated according to the standard finite element approximation as,

$$\phi^h(\boldsymbol{x},t) = \sum_{A=1}^{n_s} N^A(\boldsymbol{x})\,\phi^A(t) \tag{22}$$

Discretization of governing equations

The spatially discretized form of the variational or weak form for establishing the unknown fields $c_i^h \in \mathcal{C}^h$ ($i = \{1,2,3,4\}$) and $\psi^h \in \Psi^h$ are given as:

$$\int_{\Gamma_{int}} w^h \frac{1}{L_0}\boldsymbol{j}_i^h \cdot \boldsymbol{n}\,\mathrm{d}\Omega - \int_{\Omega_l} \nabla w^h \cdot \left(\nabla c_i^h + \nabla\psi^h z_i c_i^h\right)\mathrm{d}\Omega = 0 \tag{23}$$

$$\int_{\Omega_l \cup \Gamma_{int}} w^h \sum_{i=1}^{4} \frac{D_0 c_i^h z_i}{D_i}\,\mathrm{d}\Omega = 0 \tag{24}$$

$$\int_{\Gamma_{int}} u^h \frac{1}{L_0}\boldsymbol{j}_\psi^h \cdot \boldsymbol{n}\,\mathrm{d}\Omega - \int_{\Omega_l} \nabla u^h \cdot \sum_{i=1}^{4}\left(z_i\nabla c_i^h + z_i^2 c_i^h \nabla\psi^h\right)\mathrm{d}\Omega = 0 \tag{25}$$

where the weighting functions w^h and u^h are also discretized according to the extended finite element approximation, $\mathcal{C}^h$ and Ψ^h are discretized finite element functional spaces. The residual vector $\boldsymbol{R}^A = \{R_i^A\}, i = \{1,2,3,4,5\}$ at a standard finite element node A corresponding to the five equations (23)–(25) in five unknowns is given as,

$$R_i^A = -\int_{\Omega_l} \nabla N^A \cdot \nabla c_i^h\,\mathrm{d}\Omega - \int_{\Omega_l} \nabla N^A \cdot \left(\nabla\psi^h z_i c_i^h\right)\mathrm{d}\Omega + \int_{\Gamma_{int}} N^A \frac{1}{L_0}\boldsymbol{j}_i^h \cdot \boldsymbol{n}\,\mathrm{d}\Omega, \qquad i = \{1,2,3\} \tag{26}$$

$$R_4^A = \int_{\Omega_l \cup \Gamma_{int}} N^A \sum_{i=1}^{4} \frac{D_0 c_i^h z_i}{D_i}\,\mathrm{d}\Omega \tag{27}$$

$$R_5^A = -\sum_{i=1}^{4}\int_{\Omega_l} \nabla N^A \cdot z_i \nabla c_i^h\,\mathrm{d}\Omega - \sum_{i=1}^{4}\int_{\Omega_l} \nabla N^A \cdot z_i^2 c_i^h \nabla\psi^h \mathrm{d}\Omega + \int_{\Gamma_{int}} N^A \frac{1}{L_0}\boldsymbol{j}_\psi^h \cdot \boldsymbol{n}\,\mathrm{d}\Omega \tag{28}$$

Let us assume that, at a given time t all the five unknown fields are known at iteration k and sought at the next iteration $k+1$ at any finite element node A as given by,

$$\begin{aligned} {}^{k+1}c_i^A &= {}^{k}c_i^A + \Delta c_i^A \\ {}^{k+1}\psi^A &= {}^{k}\psi^A + \Delta\psi^A \end{aligned} \tag{29}$$

where Δc_i^A and $\Delta\psi^A$ are the corresponding increments. Assuming that the residual vector $\boldsymbol{R}^A$ can be linearized for small increments in the unknown field vector $\boldsymbol{y} = \{c_1, c_2, c_3, c_4, \psi\}$, the expression for the residual at the next iteration $k+1$ is written using Taylor's expansion as,

$$0 = {}^{k+1}R_i^A = {}^{k}R_i^A + \left[\frac{\partial R_i^A}{\partial y_j^B}\right]\Delta y_j^B \tag{30}$$

Rewriting the above equation into a fully discretized and linearized system of equations, one obtains,

$$K_{ij}^{AB}\Delta y_j^B = -\,{}^{k}R_i^A \tag{31}$$

where K_{ij}^{AB} is the numerical approximation of the consistent tangent matrix defined as,

$$K_{ii}^{AB} = \left[\frac{\partial R_i^A}{\partial c_i^B}\right] = \int_{\Omega_l} \nabla N^A \cdot \nabla N^B\,\mathrm{d}\Omega + \int_{\Omega_l} \nabla N^A \cdot \left(\nabla\psi^h z_i\right) N^B \mathrm{d}\Omega,\ i = \{1,2,3\} \tag{32}$$

$$K_{i5}^{AB} = \left[\frac{\partial R_i^A}{\partial \psi^B}\right] = \int_{\Omega_l} \nabla N^A \cdot \left(c_i^h z_i\right)\nabla N^B \mathrm{d}\Omega, \qquad i = \{1,2,3\} \tag{33}$$

$$K_{4i}^{AB} = \left[\frac{\partial R_4^A}{\partial c_i^B}\right] = -\int_{\Omega_l} N^A \cdot \frac{D_0 z_i}{D_i} N^B\,\mathrm{d}\Omega \tag{34}$$

$$K_{5i}^{AB} = \left[\frac{\partial R_5^A}{\partial c_i^B}\right] = \int_{\Omega_l} \nabla N^A \cdot z_i \nabla N^B\,\mathrm{d}\Omega + \int_{\Omega_l} \nabla N^A \cdot z_i^2 N^B \nabla\psi^h \mathrm{d}\Omega, i = \{1,2,3,4\} \tag{35}$$

$$K_{55}^{AB} = \left[\frac{\partial R_5^A}{\partial \psi^B}\right] = \sum_{i=1}^{4}\int_{\Omega_l} \nabla N^A \cdot z_i^2 c_i^h \nabla N^B\,\mathrm{d}\Omega \tag{36}$$

The procedure to derive the system tangent is similar even for an enriched element, except that the unknown vector field vector $\boldsymbol{y} = \{c_1, c_2, c_3, c_4, \psi, a_1, a_2, a_3, a_4, \xi\}$ contains additional enriched degrees of freedom and the corresponding residual vector is defined as, $\boldsymbol{R}^B = \{R_i^B\}, i = \{1,2\ldots,10\}$, where the additional terms at enriched node B are given by,

$$R_i^B = -\int_{\Omega_l} \nabla S^B \cdot \nabla c_i^h \, \mathrm{d}\Omega - \int_{\Omega_l} \nabla S^B \cdot \left(\nabla \psi^h z_i c_i^h\right) \mathrm{d}\Omega + \int_{\Gamma_{int}} S^B \frac{1}{L_0} \boldsymbol{j}_i^h \cdot \boldsymbol{n} \, \mathrm{d}\Omega, \qquad i = \{6,7,8\} \tag{37}$$

$$R_9^B = \int_{\Omega_l \cup \Gamma_{int}} S^B \sum_{i=1}^{4} \frac{D_0 c_i^h z_i}{D_i} \, \mathrm{d}\Omega \tag{38}$$

$$R_{10}^B = -\int_{\Omega_l} \nabla S^B \cdot z_i \nabla c_i^h \, \mathrm{d}\Omega - \int_{\Omega_l} \nabla S^B \cdot z_i^2 c_i^h \nabla \psi^h \, \mathrm{d}\Omega + \int_{\Gamma_{int}} S^A \frac{1}{L_0} \boldsymbol{j}_\psi^h \cdot \boldsymbol{n} \, \mathrm{d}\Omega \tag{39}$$

For more details on obtaining the specific expression of the consistent tangent K_{ij}^{AB} for the standard and enriched finite element approximations, the reader is referred to [8].

NUMERICAL RESULTS

In this section, the viability of the extended finite element formulation is demonstrated for simulating intergranular crevice corrosion in AA5083 alloys. Two numerical examples are set up with domain configurations corresponding to: (1) *crevice corrosion at time* $t = 0^+$, wherein the Mg phase begins to dissolve into aqueous solution; and (2) *crevice corrosion at time* $t > 0^+$, wherein a significant portion of the Mg phase in the intergranular crevice has dissolved and the side walls of the crevice expose the Al phase in the grains (see Figure 1).

Model parameters

The Nernst-Planck model parameters including the Fickian diffusion coefficients and the far field concentrations of the ionic species in aqueous solution, and the universal constants are given in Table 1. The electrochemical properties for AA5083 corrosion in 0.5M NaCl solution are listed in Table 2. The forward Tafel slopes for the electrode reactions are obtained from [25] and then the reverse Tafel slopes are calculated assuming Butler-Volmer kinetic relations as [26],

$$\alpha_a = 2.303 \frac{RT}{z_1 F \beta_{af}}; \beta_{ar} = 2.303 \frac{RT}{z_1 F (1 - \alpha_a)}$$
$$\alpha_c = 2.303 \frac{RT}{z_2 F \beta_{cf}}; \beta_{ar} = 2.303 \frac{RT}{z_2 F (1 - \alpha_c)} \tag{40}$$

where α_a and α_c are the so-called anodic and cathodic charge transfer coefficients.

Parameter	Value (units)
F	96485.3 C/mol
R	8.314 J/mol/K

T	25 °C
z_1	+2
z_2	−1
z_3	−1
z_4	+1
D_1	7.05×10^{-10} m^2/s
D_2	5.27×10^{-9} m^2/s
D_3	1.33×10^{-9} m^2/s
D_4	2.03×10^{-9} m^2/s
C_1^∞	3×10^{-4} mol/m^3
C_2^∞	6×10^{-4} mol/m^3
C_3^∞	500 mol/m^3
C_4^∞	500 mol/m^3
D_0	5.27×10^{-9} m^2/s
C_0	6×10^{-4} mol/m^3

Table 1. Model parameters for ion diffusion in aqueous solution. The Fickian diffusion coefficients D_i of ions at infinite dilution at 25 °C in seawater are obtained from [27]. The far field concentrations c_i^∞ are assumed from [18] and [25].

	Γ_a	Γ_c
ϕ_o	−1.25 V	−0.7 V
i_o	10^{-5} A/m^2	10^{-5} A/m^2
β_f	0.137 V/dec	−0.234 V/dec
β_r	−0.0377 V/dec	0.0792 V/dec

Table 2. Electrochemical properties for AA5083 corrosion. The open-circuit potentials and corrosion current densities are taken from [18]. The forward and reverse Tafel slopes obtained from electrochemical frequency modulation (EFM) technique at 0.01 Hz are taken from [25]. The reverse Tafel constants are calculated according to equation (40).

Example 1: Crevice corrosion at time $t = 0^+$

Let us consider the intergranular crevice corrosion problem at time $t = 0^+$. A key assumption is that interface evolution due to corrosive dissolution is much slower compared to ion transport, so the ionic concentrations c_i are assumed to be at steady state at time $t = 0^+$; this assumption is reasonable given the timescales of ion diffusion and corrosive dissolution [18]. The rectangular domain is 0.042 mm × 42 mm (width × height) and consists of two Al grains 0.020 mm × 0.021mm with an intergranular crevice 0.002 mm × 0.021 mm, similar to that in Sarkar et al., [18]. The interface Γ_{int} divides the domain into two halves and is initialized as,

$$\phi(\boldsymbol{x}, 0) = x_2 - 0.021 \text{ mm} \quad \forall \ \boldsymbol{x} \in \Omega \tag{41}$$

where $\boldsymbol{x} = (x_1, x_2)$ are the Cartesian coordinates. The interface Γ_{int} can now be captured by the zero contour of the level set

function $\phi(\boldsymbol{x}, t)$ at anytime. The cathode and anode segments of the interface are determined depending on whether a particular interface segment corresponds to the exposed surface of the Al phase or Mg phase as,

$$\Gamma_a(t) = \{\boldsymbol{x} \in \Omega |\ \phi(\boldsymbol{x}, t) = 0\ \&\ f^s(\boldsymbol{x}) = 0\} \tag{42}$$

$$\Gamma_c(t) = \{\boldsymbol{x} \in \Omega |\ \phi(\boldsymbol{x}, t) = 0\ \&\ f^s(\boldsymbol{x}) = 1\} \tag{43}$$

where $f^s(\boldsymbol{x})$ denotes the value of the volume fraction variable when the interface is approached from the solid domain Ω_s. The configuration of the alloy-electrolyte domain and domain boundaries is shown below in Figure 2.

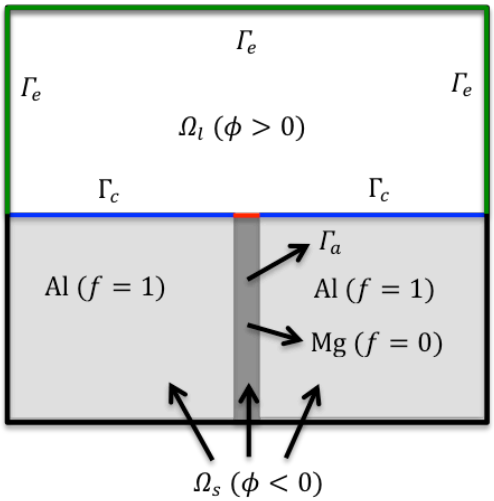

Figure 2. Schematic diagram of the intergranular crevice corrosion problem in AA5083 at initial time $t = 0$. The interface described by the level set function is partitioned into the cathodic (blue) and anodic (red) segments depending on whether it corresponds to the Al phase or Mg phase.

The domain Ω is discretized using a square bilinear finite element mesh containing 101 × 101 elements. About 4 to 8 Netwon-Raphson iterations were required by the solver to obtain convergence. The simulation results for the concentrations of Mg^{2+}, Cl^-, Na^+ along with the pH $(= 14 + \log_{10}[OH^-])$ of the solution are shown in Figure 3. Notice the discontinuity in concentration and its flux across the interface at $x_2 = 0.021$ mm in Figures 3(a)–3(d). The XFEM allows for the incorporation these discontinuities via the step enrichment of the standard finite element shape functions. These results have been compared with those obtained from commercial software COMSOL Version 4.2 using the chemical engineering module and the error was within acceptable tolerance (less than 3–4%) for a similar number of degrees of freedom. However, it is to be noted that an unstructured finite element mesh with triangular elements was employed in COMSOL analysis; whereas, a structured mesh with square-shaped bilinear elements was used in XFEM analysis. This benchmark investigation establishes the validity and viability of the proposed extended finite element formulation.

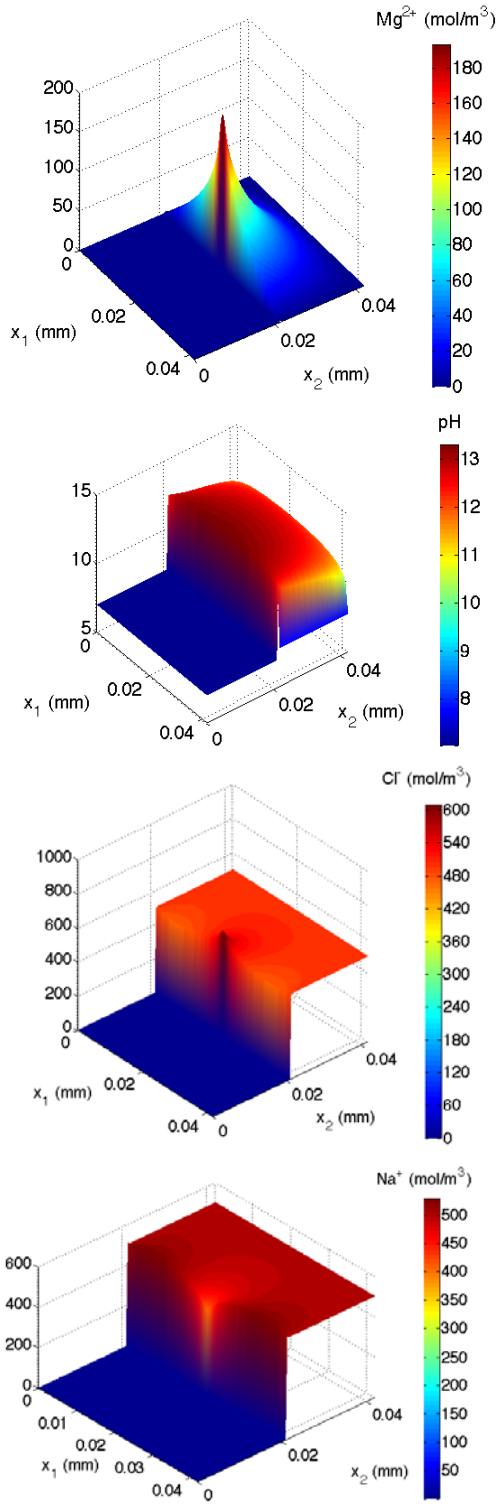

Figure 3. Model predicted concentration of ionic species in solution at time $t = 0^+$. These results were validated with those obtained from COMSOL Version 4.2. Notice the discontinuity in concentration and the corresponding fluxes across the interface at $x_2 = 0.021$ m.

The results shown in Figure 3 indicate that, since Mg phase is anodic with respect to the Al phase, Mg dissolves into solution as Mg^{2+} ions causing a spike in its concentration locally around the anode boundary Γ_a. To maintain electro-neutrality Cl^- ions migrate towards Γ_a and Na^+ ions migrate away from Γ_a. The pH of the solution reaches a value of 13 in the vicinity of the interface, indicating that the solution becomes highly alkaline as soon as dissolution begins. However, this may not be an accurate description of the crevice environment as the concentration of OH^- and Mg^{2+} ions is regulated by the precipitation of $Mg(OH)_2$. This suggests it is essential to account for chemical reactions (precipitation), which will be studied in a future modeling focused paper. It is evident from Figure 4 that the model predicted electrolyte potential φ is on the order of millivolts and is much smaller than the open circuit potentials φ_{oa} and φ_{oc}. However, the trends of a positive voltage near the anode and negative voltage near the cathode in Figure 4 seem to be in general agreement with theory.

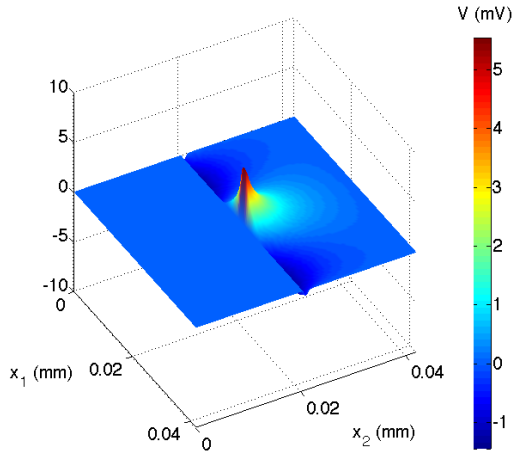

Figure 4. Model predicted electrical potential φ in the solution at time $t = 0^+$

Example 2: Crevice corrosion at time $t > 0^+$

Let us now consider the intergranular crevice corrosion problem at a later time $t > 0^+$ when the Mg phase in the grain boundary has dissolved to a depth of $x_2 = 10\,\mu$m. Consequently, the cathode boundary is now larger than before due to the creation of the newly exposed crevice sidewalls; whereas, the anode boundary length is the same. The configuration of the alloy-electrolyte domain and domain boundaries are schematically illustrated in Figure 1. Since in the current XFEM and level set based sharp-interface model formulation the interface can be represented independent of the underlying finite element mesh, the same finite mesh can be used at all times, as shown in Figure 5. The results for this configuration are shown in Figures 6 and 7.

The results indicate similar trends in concentrations and electrical potential as in the previous example. As expected, the concentration of Mg^{2+} ions is significantly larger in the crevice environment because the ion diffusion path is longer, which turn causes a more aggressive migration of Cl^- ions into the intergranular crevice in order to maintain electro-neutrality. The maximum value of pH in the solution seems to be more than 13 indicating that the crevice environment is highly alkaline. We again note that this may not be the realistic case because chemical reactions and precipitation was neglected in this preliminary model. The electrical potential in the crevice still seems to be generally small (about a few millivolts). While this study establishes the computational prowess of the proposed formulation, an improved mathematical model would be necessary to simulate the electrochemistry of galvanic corrosion in AA5083 alloys.

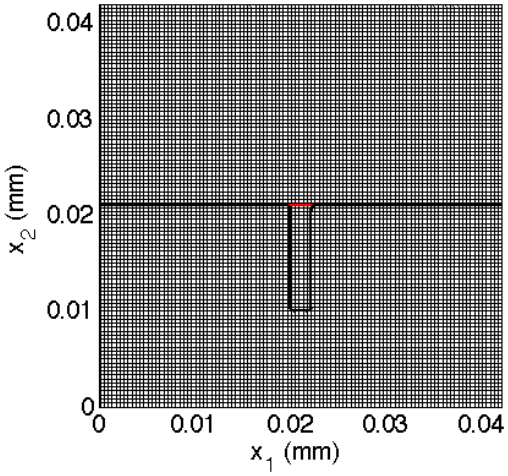

Figure 5. Finite element mesh containing 101 × 101 square bilinear elements can be used for analysis at all times. The initial interface (red) and the interface at a subsequent time (black) are defined by the zero contour of the level set function. Thus, the proposed formulation entirely eliminates the need for remeshing or mesh moving procedures.

CONCLUSION

In this paper, a new extended finite element model formulation was developed for investigating crevice and pitting corrosion in alloys. The non-dimensionalization scheme for the governing equations of the model, namely, the Nernst-Planck equations along with the electro-neutrality condition for ion diffusion in dilute electrolyte solution, improves numerical convergence. The level set representation of the interface and the step enrichment of the finite element basis allow the simulation of arbitrary crevice geometries using a structured finite element mesh without needing remeshing; this would be a significant advantage, especially, when the interface is evolved in time during a corrosion propagation simulation. Numerical results are in good agreement with those obtained from COMSOL Version 4.2 chemical engineering module, which demonstrates the viability of the proposed formulation.

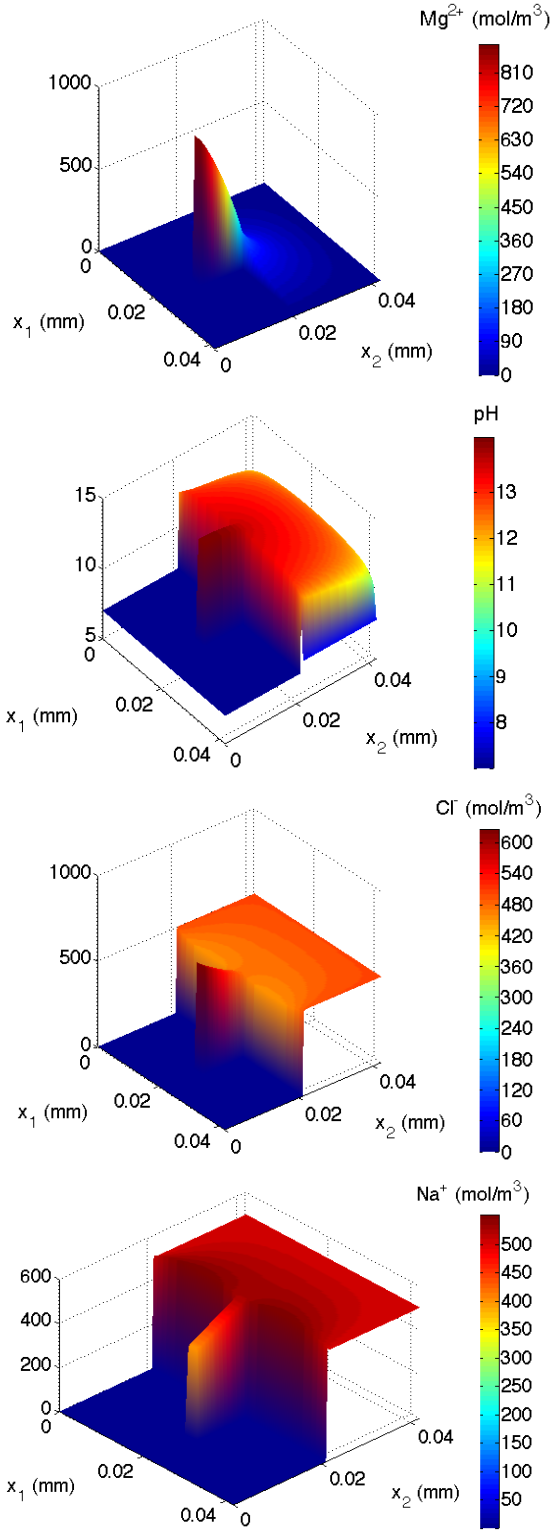

Figure 6. Model predicted concentration of ionic species in solution at time $t > 0^+$, when the intergranular crevice is about 0.011 mm long. Notice the discontinuity in concentrations and the corresponding fluxes across the arbitrary crevice interface.

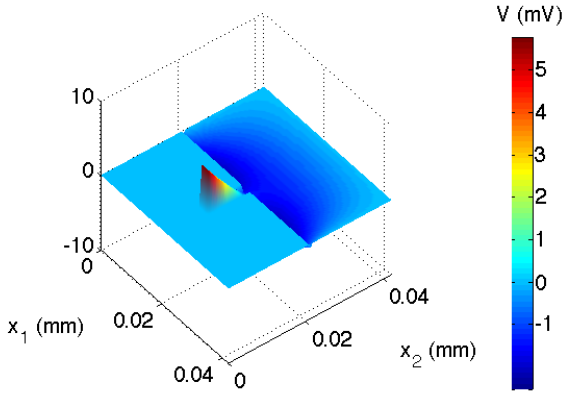

Figure 7. Model predicted electrical potential φ in the solution at time $t > 0^+$. The potential is on the order of millivolts and is positive in the intergranular crevice and is negative at the cathodic boundaries at $x_2 = 0.021$ mm.

Since the model is based on the dilute solution theory for ion diffusion it is able to predict the qualitative behavior of ion migration in the liquid domain, such as, the migration of chloride ions into crevices and pits from the bulk solution [28]. The increased presence of chloride ions near the Mg (anode) surface can accelerate the corrosion process, as noted by Song and Atrens [28]. The model also predicts an increase in the pH (i.e., alkalinity) of the solution environment, which would reduce the rate of dissolution since magnesium is very resistant to corrosion by alkalis, especially, when the pH > 10.5 [28]. However, since the reaction associated with $Mg(OH)_2$ formation is ignored, the model may not be representing the chemical environment in the crevice, quantitatively, as evident from the is unrealistically high pH predicted in the solution domain. Moreover, it seems like the assumptions of the dilute solution theory may not be valid everywhere in the domain. In conclusion, while this model is an improvement over the too simplistic Fickian diffusion model, it has some major limitations in its current form.

Model validation using experimental data in the literature is currently difficult due to the lack of high-resolution in situ techniques [29] that can provide microscale information comparable to simulation results; however, a detailed review of experimental and modeling studies on magnesium corrosion can be found in [30]. Our future work will focus on formulating models for corrosion in concentrated solutions, incorporating the chemical reaction associated with $Mg(OH)_2$ formation, the time evolution of the anode and cathode interfaces, validating with experimental data, and uncertainty quantification of corrosion rates.

ACKNOWLEDGMENTS

The authors gratefully acknowledge the financial support of the Office of Naval Research (ONR) Summer Faculty Fellowship Program.

REFERENCES

[1] Hoeppner DW, Taylor AMH (2011) AVT-140 Corrosion fatigue and environmentally assisted cracking in aging military vehicles. Chapter 13. Modeling pitting corrosion fatigue: Pit growth and Pit/Crack transition issues. NATO, RTO, France.

[2] Scully JC (1990) The fundamentals of corrosion, 3rd edn. Pergamon Press, New York

[3] Sharland SM, Jackson CP, Diver AJ (1989) A finite-element model of the propagation of corrosion crevices and pits. Corros. Sci. 29(9):1149–1166

[4] Alkire R, Siitari D (1979) The location of cathodic reaction during localized corrosion. J Electrochem Soc 126(1):15–22

[5] Laycock NJ, White SP, Noh JS, Wilson PT and Newman RC (1998) Perforated covers for propagating pits. J Electrochem Soc 145(4):1101–1108

[6] Scheiner S, Hellmich C (2007) Stable pitting corrosion of stainless steel as diffusion-controlled dissolution process with a sharp moving electrode boundary. Corros Sci 49(2):319–346

[7] Scheiner S, Hellmich C (2009) Finite volume model for diffusion and activation-controlled pitting corrosion of stainless steel. Comput Method Appl Mech Eng 198(37–40):2898–2910

[8] Duddu R (2014) Numerical modeling of corrosion pit propagation using the combined extended finite element and level set method." Comput. Mech. 54(3): 613–627

[9] Sharland SM, Tasker PW (1988) A mathematical model of crevice and pitting corrosion – I. The physical model. Corros Sci 28(6):603–620

[10] Sharland SM (1988) A mathematical model of crevice and pitting corrosion – II. The mathematical solution. Corros Sci 28(6):621–630

[11] Walton JC (1990) Mathematical modeling of mass transport and chemical reaction in crevice and pitting corrosion. Corros Sci 30(8/9):915–928

[12] Malki B, Souier T, Baroux B (2008) Influence of the alloying elements on pitting corrosion of stainless steels: A modeling approach. J. Electrochem. Soc. 155(12):C583–C587

[13] Oltra R, Malki B, Rechou F (2010) Influence of aeration on the localized trenching on aluminum alloys. Electrochim Acta 55(15): 4536–4532

[14] Xiao J, Chaudhuri S (2011) Predictive modeling of localized corrosion: an application to aluminum alloys. Electrochim Acta 56(24):5630–5641

[15] Sarkar S, Aquino W (2011) Electroneutrality and ionic interactions in the modeling of mass transport in dilute electrochemical systems. Electrochim Acta 56(16):8969–8978

[16] Sarkar S, Warner JE, Aquino W (2012) A numerical framework for the modeling of corrosive dissolution. Corros Sci 65:502–511

[17] Sarkar S, Aquino W (2013) Changes in electrodic reaction rates due to elastic stress and stress-induced surface patterns. Electrochim Acta 11(16):814–822

[18] Sarkar S, Warner JE, Aquino W, Grigoriu MD (2014) Stochastic reduced order models for uncertainty quantification of intergranular corrosion rates. Corros Sci 80:257–268

[19] Laycock NJ, White SP (2001) Computer simulation of single pit propagation in stainless steel under potentiostatic control. J Electrochim Soc 148(7):B264–B275

[20] Vagbharathi AS and Gopalakrishnan S (2014) An extended finite element model coupled with level set method for analysis of growth of corrosion in pits in metallic structures. Proc. R. Soc. A 470:20140001

[21] Chen Z, Bobaru F (2015) Peridynamic modeling of pitting corrosion damage, J. Mech. and Phys. Solids, 78:352–381

[22] Belytschko T, Black T (1999) Elastic crack growth in finite elements with minimal remeshing. Int J Numer Method Eng 45:601–620

[23] Moës N, Dolbow J, Belytschko T (1999) A finite element method for crack growth without remeshing. Int J Numer Method Eng 6(1):131–150

[24] Sethian JA (1999) Level set methods & fast marching methods: evolving interfaces in computational geometry, fluid mechanics, computer vision, and materials science. Cambridge University Press, Cambridge

[25] Kus S, Mansfeld F (2006) An evaluation of the electrochemical frequency modulation (EFM) technique, Corros. Sci. 48:965–979

[26] Laycock NJ, Newman RC (1998) Temperature dependence of pitting potentials for austenitic stainless steels above their critical pitting temperature. Corros Sci 40(6):887–902

[27] Li Y-H, Gregory S (1974) Diffusion of ions in seawater and in deep-sea sediments. Geochim. Et Cosmochim. Acta 38:703–714.

[28] Song GL, Atrens A (1999) Corrosion mechanisms of magnesium alloys. Adv. Engrg. Mat. l: 11-33.

[29] Song GL (2014) The grand challenges in electrochemical corrosion research. Front. Mater. 1: 00002.

[30] Atrens A, Song GL, Liu M, Shi Z, Cao F, Dargusch MS (2015) Review of recent developments in the field of magnesium corrosion. Adv. Engrg. Mat. 17(4):400–453.